POWER-LAW DISTRIBUTIONS OF PARTICLE CONCENTRATIONS IN FREE-SURFACE TURBULENCE

by

Jason M. Larkin

B.S. Mechanical Engineering, University of Pittsburgh, 2007

Submitted to the Graduate Faculty of

the Swanson School of Engineering in partial fulfillment

of the requirements for the degree of

Master of Science

University of Pittsburgh

2009

UNIVERSITY OF PITTSBURGH

SWANSON SCHOOL OF ENGINEERING

This thesis was presented

by

Jason M. Larkin

It was defended on

July 17, 2009

and approved by

Walter I. Goldburg, Ph.D., Professor Emeritus of Department of Physics and Astronomy

Sung Kwon Cho, Ph.D., Assistant Professor of Mechanical Engineering and Materials

Science

Bong Jae Lee, Ph.D., Assistant Professor of Mechanical Engineering and Materials Science

Thesis Advisor: Walter I. Goldburg, Ph.D., Professor Emeritus of Department of Physics and

Astronomy

POWER-LAW DISTRIBUTIONS OF PARTICLE CONCENTRATIONS IN FREE-SURFACE TURBULENCE

Jason M. Larkin, M.S.

University of Pittsburgh, 2009

Particles floating on the surface of an incompressible turbulent fluid cluster into intermittent, complex structures. This system is studied experimentally by analyzing the statistics of the coarse-grained particle concentration, c_r, as a function of scale r, in both the inertial and dissipative regimes of the turbulent field. The first moment of the concentration c_r exhibits scale-free dependence on the coarse-graining scale r in both the inertial and dissipative ranges, with exponents α_i (inertial) and α_d (dissipative). The probability density function of the coarse-grained particle concentration exhibits a power-law decay over a broad range of values of the concentration: $\prod(c_r) \sim c_r^{-\beta_r}$, where β_r is approximately independent of scale in the dissipative range $\beta_r \approx 0.8 \pm 0.05$, and decreases with increasing r in the inertial range. The PDF then falls off faster than algebraically at very large values of c_r. The observed steep algebraic decay is a manifestation of the broad distribution of particle concentrations produced by surface flow upwellings (sources), which lie between very dense line-like concentrations along surface flow downwellings (sinks).

TABLE OF CONTENTS

LIST OF TABLES

LIST OF FIGURES

PREFACE

This thesis was *written* by me, but was made *possible* by many. I will try to list as many as I can, knowing that many will be left out surely. First, I would like to thank my parents. I would also like to thank my wife Jodi for keeping me encouraged at all times, and in general, putting up with me. I would like to thank Dr. A. M. Robertson and Dr. G. P. Galdi for encouragement, teaching, and guidance. I would also like to thank Dr. Robertson for introducing me to Walter, who was kind enough to take me on as a student. In the time I've spent working with him I've developed an immense enthusiasm for learning physics, for which I thank him very much. I'd like to thank those who have come and gone through Walter's lab during my time, in particular Stanley Steers (for his enthusiasm), Alisia Prescott (for helping with my experiments), and Tuan Tran for his insight and dedication.

I'd very much like to thank Dr. Mahesh Bandi. His previous work and the work of Dr. Rob Cressman made this experiment enjoyable, and dare I say, "easy". Furthermore, his technical and personal guidance have been top-notch, honest, and with great humility. Interacting with him has been more valuable than he may know. Alongside Mahesh I must also thank Dr. Alain Pumir. In working with him I've been witness to a truly first rate physicist. His insights and suggestions made a great deal of this work as good as it is, if not possible entirely. I'd like to thank both Dr. Cho and Dr. Lee for serving on my thesis committee. I'd like to thank the staff and various professors I've had here at Pitt, in the various classes I've taken (both

officially and unofficially). I'm sorry for the extra questions, the belabored points, but perhaps those queries had some part to play in this work, so maybe they were worth it after all? If not, well perhaps we can work something out…

1.0   INTRODUCTION

Turbulence is widely considered the most important unsolved problem in classical physics. This work makes no attempt to understand turbulence at its core. Rather, this work is an exploration of a particular phenomenon of a turbulent system, the motion of particles at the air-water interface of a turbulent fluid. Given the non-equilibrium nature of turbulent systems and the fantastically large number of interacting degrees of freedom, turbulence has but a few number of "exact" theories from which to interpret any results [18]. This has spurred the need for a great deal of phenomenology, numerical simulation, and dimensional arguments to study turbulent systems. Even so, there is a celebrated "exact" theory for incompressible turbulence which has driven fundamental study for almost 70 years, the Kolmogorov theory of 1941 (or K41) [18]. This K41 theory has several strict requirements, among them isotropy and homogeneity of the turbulent flow. Deviations from the K41 theory have been studied extensively, and in most practical situations the requirements of K41 are strictly violated.

The system studied here is no different; there is no "exact" theory for compressible systems, let alone the compressible free-surface turbulence in this work. Therefore, this study is in the spirit of many other works in turbulence which deals with explicit departures from the K41 theory. In this experiment, buoyant particles floating on the surface of an incompressible turbulent fluid cluster into intermittent, complex structures. This system is studied by analyzing the statistics of the coarse-grained particle concentration, c_r, as a function of scale r, in both the

inertial and dissipative regimes of the turbulent field. Before discussing the experiment further, it is important to define some common turbulent parameters which will be used in the analysis to follow.

1.1   TURBULENT PHENOMENOLOGY

1.1.1   Turbulent Length Scales

There will be several turbulent parameters borrowed from the K41 theory which will be useful in interpreting the results of this work. These parameters will be discussed here. The specific details of K41 will not be discussed here, but are contained in almost any textbook on turbulence [18,25]. The reader may be confused as to why these parameters should be used to analyze this particular system, which explicitly departs from the requirements of K41. The reader is urged to read [5] for experiments and [6] for simulations studying this free-surface flow and the many similarities it has to K41 theory (and also the ways in which it departs).

Perhaps the most important phenomelogical device used in studying turbulence is the analysis of specific length scales. The two most important length scales are the largest and smallest scales of the turbulent motion, the integral and dissipative scales, respectively. The integral scale, l_0, is defined as:

$$\ell_0 = \int dr \frac{\langle v_{||}(x+r)v_{||}(x)\rangle}{\langle (v_{||}(x))^2\rangle} \tag{1}$$

Here, $v_{||}(x)$ is the component of the velocity vector which is parallel to a line drawn between two points in space of length r. The brackets denote an ensemble average over all points

2

in space. One can think of this definition as the largest scale over which velocity fluctuations in the turbulence are correlated. The integral scale establishes the largest scale of what is called the inertial range of the flow, the range of scales over which viscosity can be neglected and inertial motion dominates. According to the K41 theory, in the inertial range velocity differences over a scale r are "rough" [18]; $\left\langle \delta v(r)^2 \right\rangle = \left\langle \left(v_{||}(x+r) + v_{||}(x) \right)^2 \right\rangle \propto r^{2/3}$, which makes theoretical treatment in this range difficult [7,20].

The smallest scale of the turbulent motion is the dissipative (or Kolmogorov) scale, defined as:

$$ \eta = \left(\frac{v^3}{\varepsilon_{diss}} \right)^{1/4} \tag{2} $$

Here, v is the kinematic viscosity of the fluid, and ε_{diss} is the energy dissipation rate [18]. The energy dissipation rate is defined as:

$$ \varepsilon_{diss} = 10v \left\langle \left(\frac{\partial v_x}{\partial x} \right)^2 \right\rangle \tag{3} $$

The brackets denote an ensemble average over space, and the factor of 10 comes from a dimensionality factor of the two-dimensional surface flow [25]. The definition of η is a dimensional argument requiring that all of the energy injected into the flow at the integral scale is dissipated due to viscosity at the dissipative scale. Hence, η is independent of the specific flow geometry or turbulent energy injection scheme and depends only on the viscosity and the rate of energy dissipation. The dissipative scale η then establishes the smallest scale of the inertial range of the flow. For length scales less than η, the flow is viscous and $\left\langle \delta v(r)^2 \right\rangle = \left\langle \left(v_{||}(x+r) + v_{||}(x) \right)^2 \right\rangle \propto r^2$, making theoretical predictions possible [7,20]. The dissipative scale will separate the analysis in this experiment which can be treated theoretically

(less than η) and that which cannot (greater than η). It is important to note that K41 is a mean field theory since it assumes that the control parameter is the *mean* energy dissipation rate and the kinematic viscosity (which is constant). Therefore, the above defined parameters are all *mean* quantities, which will also fluctuate in time and space.

An additional length scale which lies between l_0 and η is the Taylor microscale λ, defined as:

$$\lambda = \sqrt{\frac{v^2_{rms}}{\left\langle \left(\partial v_x / \partial x\right)^2 \right\rangle}} \tag{4}$$

Here, v^2_{rms} is the root mean square (RMS) velocity:

$$v_{rms} = \sqrt{\left\langle v^2 \right\rangle - \left\langle v \right\rangle^2} \tag{5}$$

The Taylor microscale lies strictly between l_0 and η as defined above.

1.1.2 Additional Turbulent Parameters

Using the above definitions, additional parameters can be defined to characterize the turbulent flow. Typically, a Reynolds number based on velocity fluctuations and a turbulent length scale is used instead of one defined by mean velocities and geometrical length scales. The Taylor microscale Reynolds number Re_λ is defined as:

$$\text{Re}_\lambda = \frac{v_{rms}\lambda}{v} \tag{6}$$

Where v is the kinematic fluid velocity, and v_{rms} and λ are defined above. This Reynolds number is typically smaller than Reynolds numbers based on flow geometries and mean velocities, but is often independent of the specific flow geometry and turbulent energy injection mechanism.

A useful time scale is the large eddy turnover time (LETT) τ_0, defined as:

$$\tau_0 = \frac{\ell_0}{v_{rms}} \tag{7}$$

This gives a quantitative measure of how long an eddy of size l_0 survives before it is removed from the flow by viscosity [18]. The final parameter which will be useful in this work is the compressibility C, defined as:

$$C = \frac{\left\langle \left(\vec{\nabla}_2 \cdot \vec{v}\right)^2 \right\rangle}{\left\langle \left(\vec{\nabla}_2 \vec{v}\right)^2 \right\rangle} \tag{8}$$

The subscript 2 on $\vec{\nabla}_2$ is meant to remind that the operator acts over only the two dimensional turbulent fluid's surface with coordinates x and y. For (2D) incompressible, isotropic flows, the compressibility lies between $C = 0$ (incompressible) and $C = 1$ (irrotational).

2.0   STATISTICS OF PARTICLE CONCENTRATION

2.1   INTRODUCTION

Understanding tracer advection in a turbulent flow is of practical interest in areas as diverse as pollutant transport, cloud formation due to inertial clustering, and dispersion of flotsam and phytoplankton at the ocean surface [1,2]. Whereas turbulent mixing and dispersion of passive tracers in incompressible flows has been studied for long [3,4], the preferential clustering of particles due to inertial effects or boundary conditions that lead to an effective compressibility has invited theoretical and experimental study only in recently [5-12].

This dissertation is concerned with the Lagrangian evolution of tracer particle concentrations at the two-dimensional air-water interface of a three dimensional turbulent flow. Although the underlying turbulence is incompressible, the tracer particles, which are lighter than water, are constrained to move only along the two-dimensional surface; they cannot follow water into the bulk. The tracers flee fluid upwellings (sources) and cluster into temporally-fluctuating string-like structures along fluid downwellings (sinks), thus forming a compressible system. It is perhaps helpful to view the coagulation phenomena in action, see Figure 2. These are actual photographs of the experiment, where the surface was initially blanketed uniformly at t=0s. The

effect of the surface flow causes the particles to concentrate along line-like structures in several fractions of a second. A simple model for this type of flow can be seen in Figure 3, where the bulk motion creates fluid sources where particles flee and sinks where particles accumulate. In the actual experiment, the locations of these sources and sinks fluctuate in time and space.

The floaters cluster due to the compressibility of the two-dimensional surface flow, quantified by the effective compressibility C (Eq. (8)). Past experiments and Direct Numerical Simulations (DNS) have consistently measured $C \approx 1/2$ at the free-surface [5]. Inertial particles, such as raindrops in a storm, cluster because they are too massive to follow the local flow in which they move [2]. In the present case, even inertia-free particles cluster because their motion is confined to the air-water interface. In both cases, the flows are effectively compressible because the particle's velocity $\vec{v}_p$ does not follow the fluid velocity exactly; $\vec{v}_p \neq \vec{v}_f$. Properties of clusters in free-surface flows thus share many similarities with their inertial counterparts [8,13]. Theoretical advances have taken advantage of these similarities. These theories [7,20] specifically exploit the statistical properties of stretching fields of fluids that exist at the smallest spatial scales (below the dissipative scale η Eq. (2)). Further progress has been made by treating the floaters as a dynamical system coupled to an incompressible turbulent reservoir [6-11]. In the inertial range of turbulence, where the velocity field is rough, theoretical guidance has proven to be difficult. The only available study comes from a surface flow model that suggests that particles cluster into multifractal distributions in both the dissipative and inertial ranges [12]. This study varied the compressibility C in numerical simulations of synthetic free-surface turbulence and quantified its effects on particle distributions. This compressibility C is not a free control parameter in this experiment

This study focuses on the concentration statistics of particle clusters as a function of the dimensionless coarse-graining scale r in the steady state (discussed in 2.2.3). The distribution of the coarse-grained concentration n_r (see 2.2.3), is very intermittent, the more so as the scale r decreases (see Figure 8). Quantitatively, intermittency can be characterized by measuring the second moment $\langle n_r^2 \rangle$ of the concentration field n_r, averaged over all points in space (Eulerian frame representation). This work will instead focus on the concentration c_r averaged over a sub-domain of size $\sim r^2$ around *each* particle in the system (Lagrangian frame representation). As explained in 2.2.3, the Eulerian and Lagrangian representations provide essentially equivalent information.

There are two main results in this work. The first concerns $\langle c_r \rangle$, the first moment of the concentration distribution, which shows two separate scaling regimes in the dissipative and inertial ranges, in qualitative agreement with [12]. Second, the probability distribution function (PDF) of the coarse-grained concentration $\prod(c_r)$ exhibits a very pronounced maximum close to $c_r = 0$. Over a large range of values of c_r, the PDF exhibits a power-law decay, $\prod(n_r) \propto c_r^{-\beta_r}$. This power-law decay reflects the highly intermittent spatial distribution of particle concentrations, Figure 8, and the strong tendency for the compressible flow to expel particles from large areas of the surface. PDFs with power-law behavior are frequently encountered in nature in many different contexts [19]. The shapes of the PDFs $\prod(c_r)$ are shown to vary systematically with scale *r*, and this evolution is quantitatively different in the dissipative and inertial ranges. The variation of the PDF's with scale *r* in the dissipative range is consistent with the theoretical predictions of a multi-fractal distribution of particles [7]. The PDFs also vary with *r* in the inertial range, leading to a multi-fractal distribution which is generally consistent with

8

the results in [12]. In section 2.2, the experimental setup, as well as the method used to evolve the Lagrangian tracer particles, will be discussed. Then, in section 2.3, the results concerning the first moment of the coarse-grained particle concentration $\langle c_r \rangle$ as well as the PDFs $\Pi(c_r, r)$, will be analyzed and discussed. This work is concluded with a discussion of the results in section 3.0
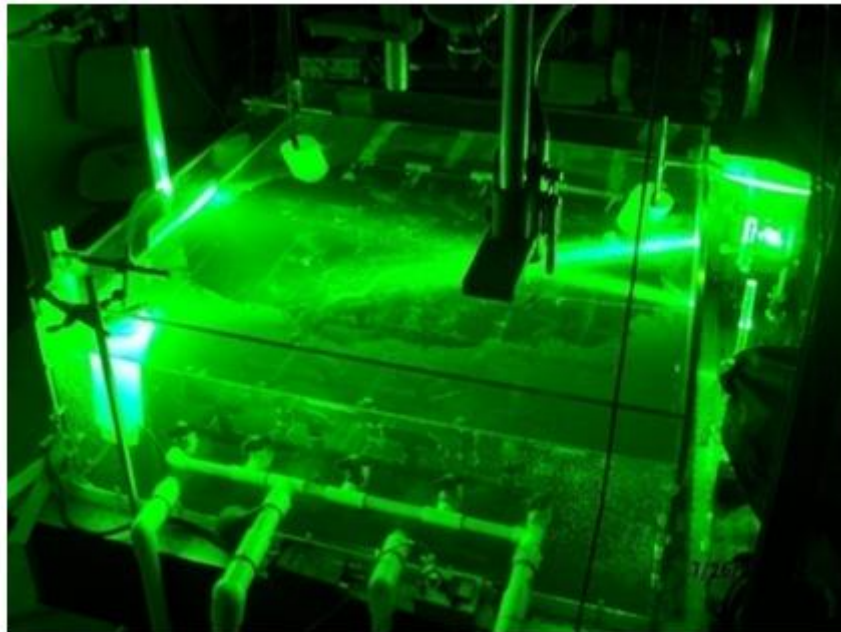

Figure 1: Photograph of experimental tank. Steady-state incompressible turbulence is created in the bulk of the tank by a grid of rotating sprinkler jets. Motion of buoyant particles at the surface are illuminated by laser and captured by a high-speed camera.
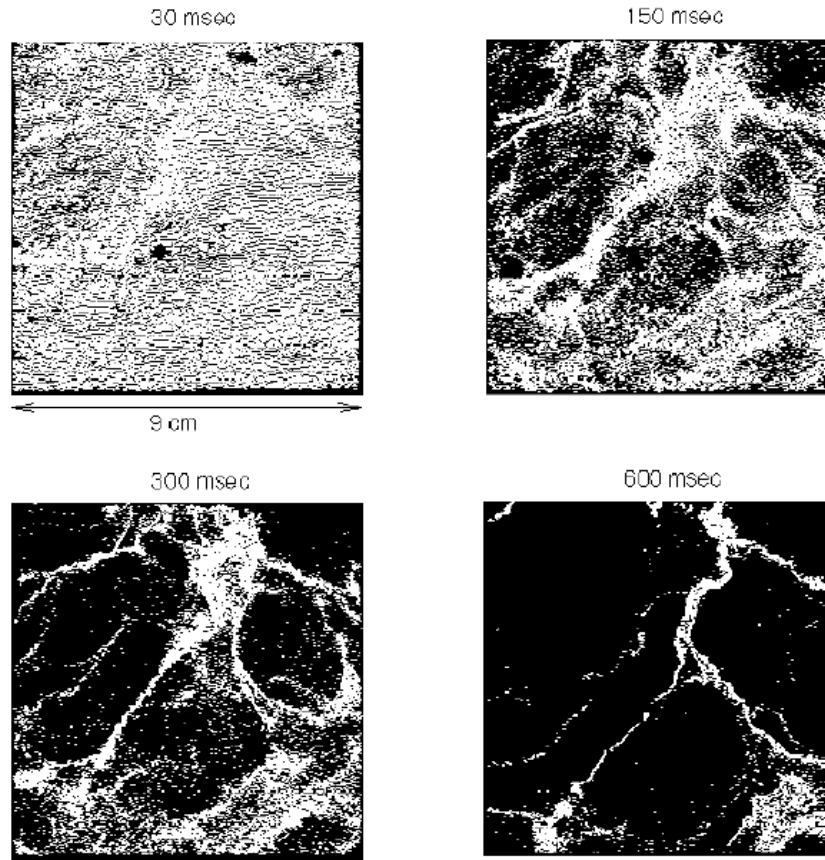
Figure 2: Photographs of the surface experiment. The evolution of particle clusters on a turbulent surface is shown for four snapshots in time as they evolve from a nearly homogeneous distribution at $t = 30$ ms towards an inhomogeneous distribution through $t = 150$ ms and 300 ms. The experiment is virtually over by $t = 600$ ms, by which time particles have almost completely clustered into string-like structures.
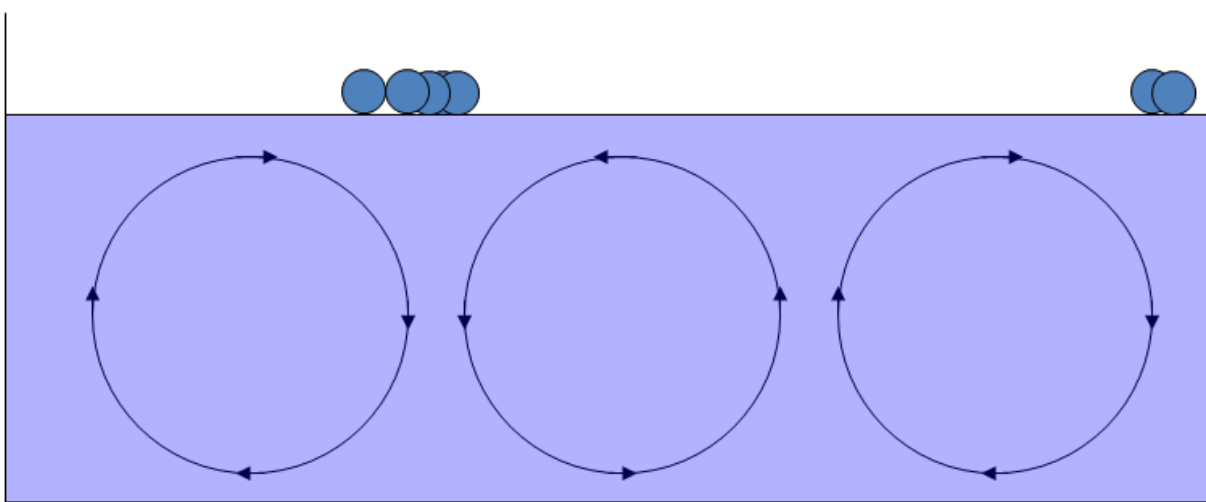
Figure 3: Simple model of surface flow. Bulk turbulent motion creates locations of fluid upwellings (sources) where particles flee and downwellings (sinks) where particles accumulate. In the actual experiment, the location of these sources and sinks fluctuates in time and space.

2.2   EXPERIMENT

2.2.1   Flow Measurements

The experiments in this work were carried out in a tank of water ($v=0.01\ cm^2/s$), $1m$ x $1m$ in lateral dimensions and filled with water to a depth of $30cm$. A schematic of this experimental setup can be seen in Figure 4: . Turbulence is generated by a pump ($8hp$) that draws water from the tank and re-circulates it through a system of 36 rotating jets placed horizontally across the tank floor. This system ensures that the source of turbulent injection is far removed from the free-surface where the measurements are made. More importantly, it minimizes the amplitude of surface waves which are unavoidable but are an additional mechanism for floater clustering that has been studied elsewhere [9]. The maximum amplitude of waves generated at the surface does

not exceed $0.5mm$ [5]. Further evidence that wave motion is not responsible for the effects reported here come from simulations where wave motion is totally absent [5]. These simulations are in very good quantitative agreement with prior laboratory experiments, where many aspects of floater coagulation were studied and compared [5].

There are several other issues to be mindful of in this experiment. First is the role of surface impurities in the form of an amphiphile layer that can cover the air-water interface. The experiment cannot be performed in the presence of these surface impurities since they suppress the coagulation seen in Figure 2. Therefore, just prior to each experimental run, the surface is cleaned by skimming off these impurities.

The second concerns the meniscus between the particles and the air-water interface and the role they play via capillary interactions, as studied in [9,14]. Particles separated by a distance comparable to their radius a will minimize their surface energy by clumping together. As a measure of the relative effects of surface tension and turbulence, a capillary number $Ca = u_\eta \mu / \gamma a$ can be defined where u_η is the Kolmogorov velocity (0.5 cm/s), μ is the dynamic viscosity of water (1 g/cm s), a is the particle radius (0.0025 cm), and γ is the surface tension of water (70 dynes/cm). Here, $Ca \approx 3$, indicating that at the dissipative scale η the turbulent fluctuations are 3 times that of the effect of surface tension. For length scales much greater than η, the relevant capillary number is $Ca = v_{rms} \mu / \gamma a$, which is much greater than 1.

Finally, as a test of the non-inertial character of the particles, their Stokes number is calculated as $St = \tau_s v_{rms} / a$, where a is the particle radius, v_{rms} is the RMS velocity of the turbulent fluid at the free-surface, and τ_s is the stopping time of the particle [11]. In order to be considered non-inertial, St for the particles must be much less than unity [15]. In the experiments discussed here, $St \cong 0.1$.

During a typical run, particles are constantly seeded into the fluid from the tank floor. They undergo turbulent mixing as they rise due to buoyancy and are uniformly dispersed by the time they rise to the surface. Once at the free-surface, their motion is constrained to the two-dimensional plane; they cannot return to the bulk. Therefore, they are expelled from the surface sources and cluster at the surface sinks. This scheme of particle injection ensures that both sources and sinks receive (nearly) equal coverage of particles on the surface. Furthermore, the constant seeding is necessary to replace any particles that leave the field of view during the experiment. A beam from a solid-state laser (5.5W) is passed through a cylindrical lens to generate a sheet of light that grazes the fluid surface. The 50μm floaters then scatter the incident laser light. The positions of the particles are captured by a high-speed camera (Phantom version 5.0), which is suspended vertically above the tank. Typically, the camera frame speed was set at 100Hz.

The high-speed camera images were stored in a computer and subsequently fed into a particle imaging velocitmetry (PIV), developed in-house. This PIV program takes a consecutive pair of images and correlates individual particles to generate an instantaneous velocity field of the turbulent surface. This special version of PIV software was developed to deal with the compressible nature of the surface flow, which naturally places a bias on particle densities around sink regions of the surface flow. This program has been checked rigorously and used in several other publications prior to this work [5,10,11]. Typically, continuous data spanning 5-10s was taken of the floaters motion at the surface, containing 500-1000 instantaneous velocity vector fields at discrete intervals in time. Figure 5 shows a visualization of a particular instantaneous velocity vector field measured during the experiment. Figure 6 shows the divergence field $\nabla \cdot \vec{v}(x, y)$ (normalized by the absolute value of the maximum divergence) for

the velocity vector field shown in Figure 5. One can clearly see the existence of sources and sinks (seen as regions of positive and negative divergence, respectively) which lead to the accumulation of particles along the string-like sinks of the flow field.

The turbulent parameters that characterize the various experimental runs in this work are calculated in. The camera field-of-view (FOV) is a square area of side length $L=9cm$. Its height above the water surface was chosen so that a pixel size is roughly $0.1mm$. This length is comparable to the dissipative scale of the turbulence. This height above the water also allows one to capture the large scale features of the coagulated floaters. The integral scale (Eq. (1)), is of the order of 1 *cm*. The high-speed camera is then able to capture the entire inertial range of the turbulent motion at the surface. Data were taken at several $Re_\lambda=150\text{-}170$ with an average $Re_\lambda \cong 160$. These data showed no systematic dependence on the Re_λ. A total of 15 independent realizations of the concentration field $n_r(t)$, separated by a large eddy turnover time τ_0, were produced from the various experimental runs. These independent runs were then used as an ensemble to produce the measurements in 2.3.
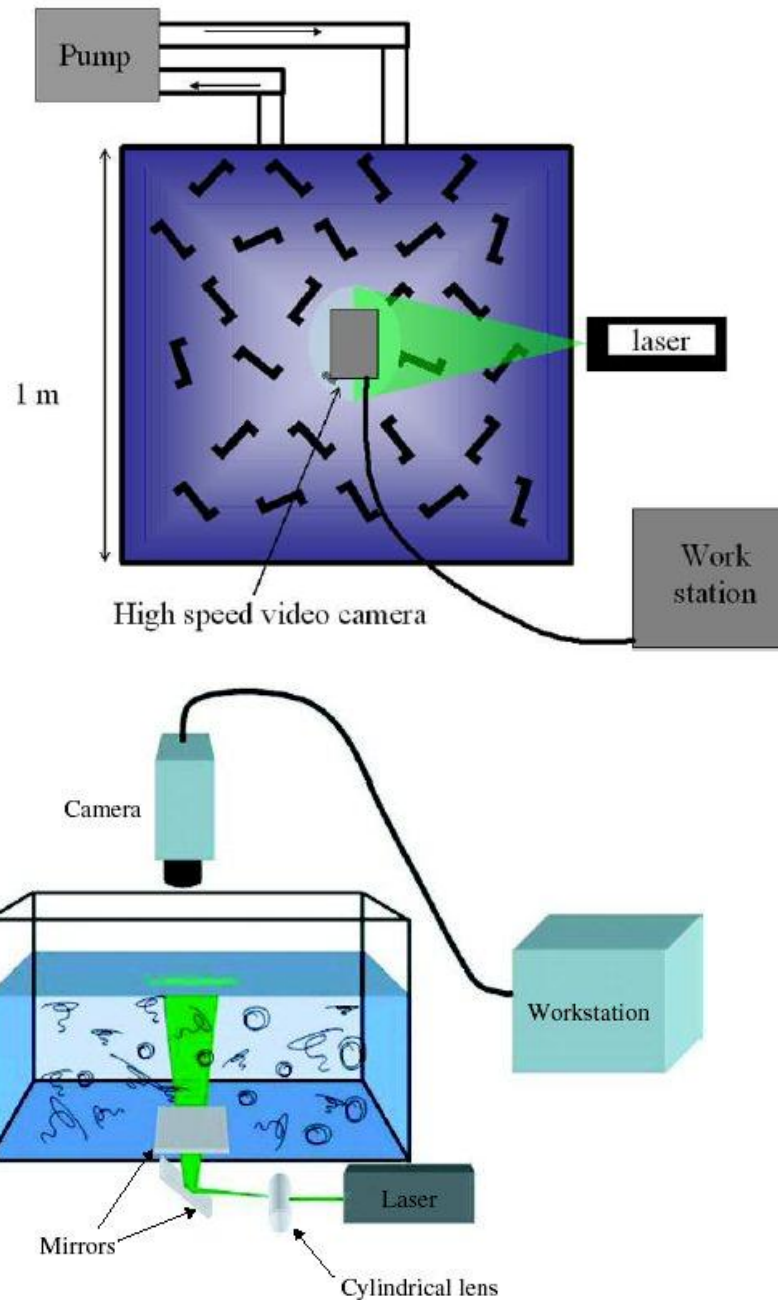
Figure 4: Schematic of the experimental setup. (Top) 36 rotating capped jets are placed horizontally on the tank floor (show in a randomly oriented Z-shaped pattern) that pumps water into the tank re-circulated by an 8hp pump. The central region of the surface is illuminated by a laser-sheet. (Bottom) A high-speed camera suspended vertically above the illuminated surface area captures images of the light scattered by the floating particles (50 μm hollow-glass spheres with specific gravity 0.25).
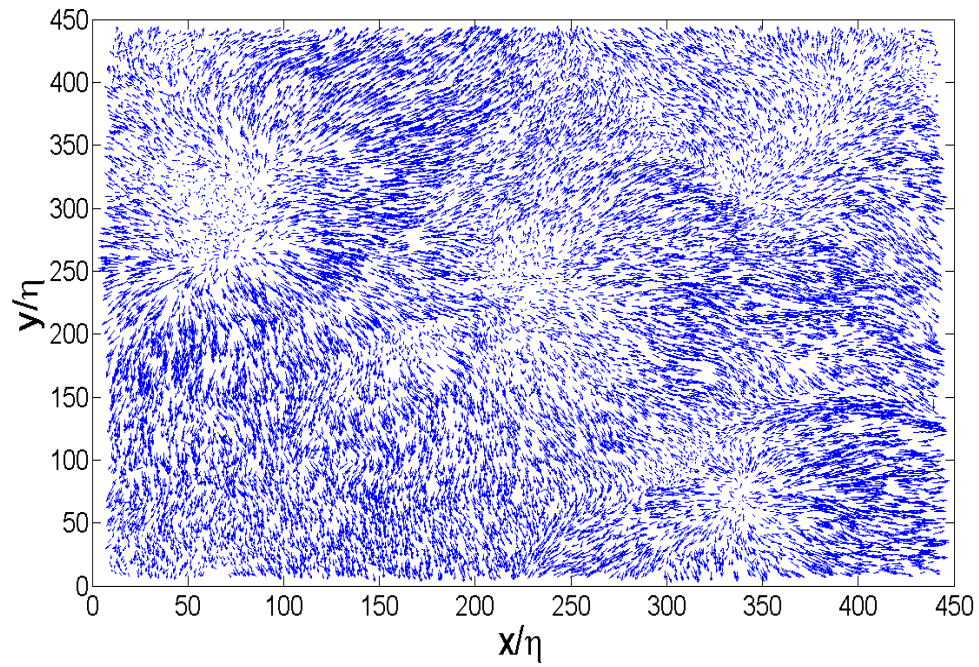
Figure 5: Visualization of the experimental velocity vector field. A snapshot of an instantaneous velocity field, as constructed by the particle tracking (PIV) program. The field is plotted in units of the spatial dimensions *x* and *y* divided by the dissipative scale *η*. A complete set of these fields spanning 5-10s are used to evolve the Lagrangian tracers.
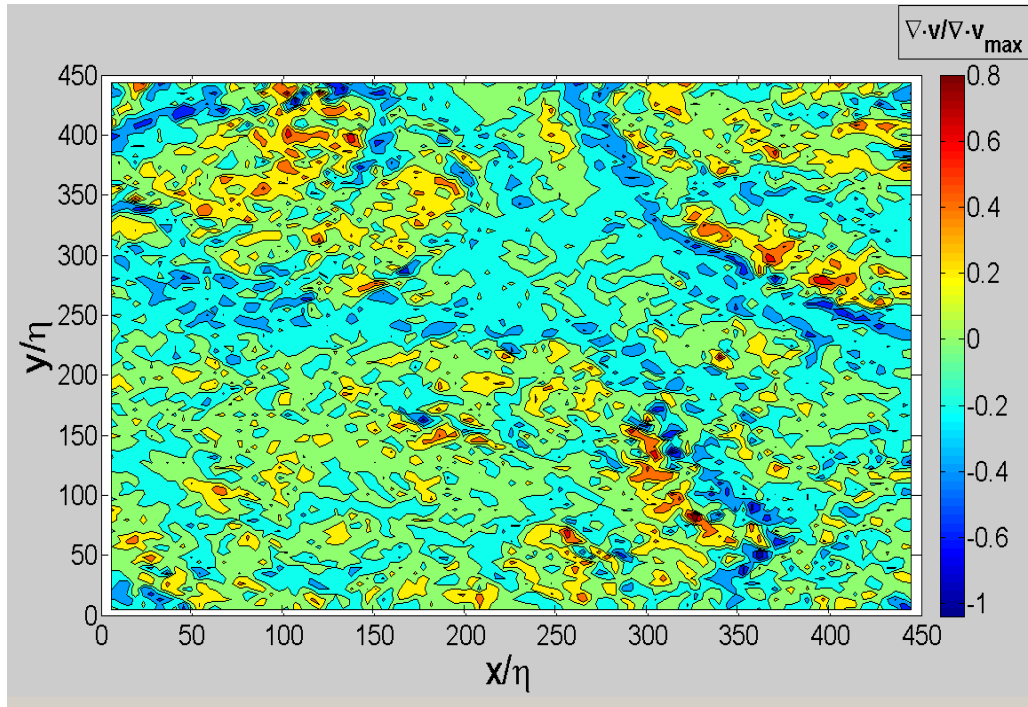
Figure 6: divergence field $\nabla \cdot \vec{v}(x, y)$**.** Visualization of a typical divergence field (normalized by the absolute value of the maximum measured divergence). The field is plotted in units of the spatial dimensions *x* and *y* divided by the dissipative scale *η*. The divergence field shows clearly the existence of fluid upwellings (sources, shown as positive divergence values) and downwellings (sinks, shown as negative divergence values).

Table 1. Turbulent parameters measured at the experiment's surface. These parameters are defined in section 1.1.

Parameter	Equation	Measured Value
Taylor microscale: λ	$\lambda = \sqrt{\dfrac{v^2_{rms}}{\left\langle (\partial v_x / \partial x)^2 \right\rangle}}$	0.46-0.47(cm)
Taylor microscale Reynolds: Re_λ	$\mathrm{Re}_\lambda = \dfrac{v_{rms}\lambda}{\nu}$	150-170
Integral Scale: ℓ_0	$\ell_0 = \int dr \dfrac{\left\langle v_\parallel(x+r)v_\parallel(x) \right\rangle}{\left\langle (v_\parallel(x))^2 \right\rangle}$	$1.45-1.5(cm)$
Large Eddy Turnover time: τ_0	$\tau_0 = \dfrac{\ell_0}{v_{rms}}$	$0.43-0.5(s)$
Energy Dissipation Rate: ε_{diss}	$\varepsilon_{diss} = 10\nu \left\langle \left(\dfrac{\partial v_x}{\partial x} \right)^2 \right\rangle$	$5.9-6.1(cm^2/s^3)$
Dissipative (Kolmogorov) length scale: η	$\eta = \left(\dfrac{\nu^3}{\varepsilon_{diss}} \right)^{1/4}$	$0.02(cm)$
RMS Velocity: v_{rms}	$v_{rms} = \sqrt{\left\langle v^2 \right\rangle - \left\langle v \right\rangle^2}$	$3.3(cm/s)$
Compressibility: C	$C = \dfrac{\left\langle (\vec{\nabla}_2 \cdot \vec{v})^2 \right\rangle}{\left\langle (\vec{\nabla}_2 \vec{v})^2 \right\rangle}$	0.49 ± 0.03

2.2.2 Particle Evolution

Once the velocity field is stored, it is then fed into a Lagrangian tracking program that solves the advection equation for a set of computer generated (massless) particles (labeled *i=1...m*) that are tracked in the Lagrangian frame of reference:

$$\frac{d\vec{x}}{dt} = \vec{v}(\vec{x}_i(t),t) \tag{9}$$

Here $\vec{v}(\vec{x}_i(t),t)$ is the velocity field and the particle coordinates (in the Eulerian frame) are labeled by $\vec{x}_i(t) = (x_i(t), y_i(t))$. To achieve sub-pixel resolution of the particle locations, as is required to measure n_r in the dissipative range, the vector field used to solve Eq. (9) was interpolated from the experimentally determined velocity fields via a cubic interpolation scheme developed for numerical simulations, as discussed in [22] and implemented in [5]. This scheme takes advantage of the smooth flow between velocity grid points which are separated by length scales comparable to the dissipative scale η to interpolate the velocity field between *measured* velocity grid points. To use this scheme it is necessary for the measured velocity grid spacing to satisfy the criterion $\delta x < \pi \eta$ [22], where δx is the average velocity field grid spacing, which is $\delta x = 2.5\eta$ in this experiment. The results presented in this work have been shown to be insensitive to the velocity grid spacing by varying $\delta x = 2.5\eta$ to $\delta x = 4\eta$.

All analysis discussed in this work is conducted on the computer generated particle tracks evolved according to Eq. (9). The real particles were only used to obtain the experimental velocity fields used in Eq. (9). Much like the *real* experiment, the *virtual* particle tracks may also extend beyond the area of the measured velocity vectors in Eq. (9). If this happens, the particle is removed from the data in the next frame and replaced by randomly re-seeding a new particle inside the experimental field of view. By extensive trial and error analysis, the minimum number

of Lagrangian particles required to perform the following analysis is approximately 10^5/frame. The statistics presented in this work was obtained by evolving ~$4\text{x}10^5$ Lagrangian particles per frame in order to ensure high statistical significance in the data. For each complete velocity field data set, a uniform distribution of Lagrangian tracers is generated at time t=0s and evolved using Eq. (9) for approximately 1.5 s, which is required for the individual moments of the concentration distribution c_r to reach a steady-state value.
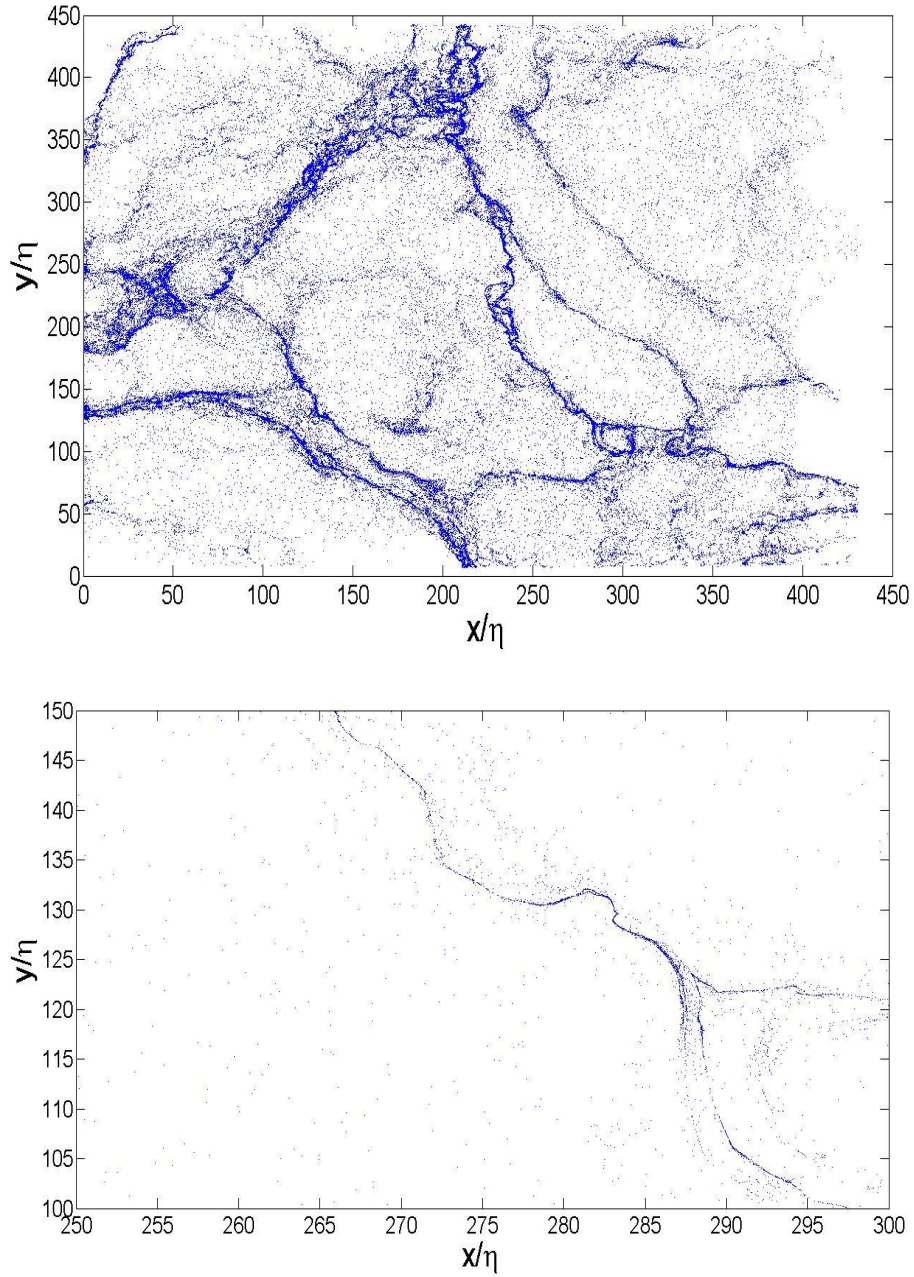
Figure 7: Visualization of the steady-state particle distribution. (Top) Resulting particle distribution at t=1.5s using the interpolation scheme described in 2.2.2. The net result of the Lagrangian particle evolution is the accumulation of high concentrations of particles along the line-like sinks, like those shown in Figure 6. (Bottom) Zoomed in view of the top figure showing structures at scales comparable to the dissipative scale η.

2.2.3 Concentration Fields: Eulerian vs. Lagrangian

The concentration statistics are collected at each time-step by coarse graining the domain at the chosen spatial scale $r=s/\eta$. Here, s is the size of the coarse-grained box in cm and η is the dissipative scale (in cm), thus making r dimensionless. The Eulerian concentration field, coarse-grained over scale r, is defined by dividing the system into square cells of size r, and by counting the number of particles $N(r,t)$ in each of them. The dimensionless Eulerian concentration is then defined as: $n_r(t) = \dfrac{N(r,t)}{\langle N(r,t) \rangle}$, where $\langle N(r,t) \rangle$ is the mean number of particles in a square of size r. This can be simply expressed in terms of the total number of particles in the system, N_t, the total size L of the system, and scale r: $\langle N(r,t) \rangle = N_t (s/L)^2$. With this definition, the mean dimensionless concentration: $\langle n_r(t) \rangle = \dfrac{\langle N(r,t) \rangle}{\langle N(r,t) \rangle} \equiv 1$.

Similarly, the Lagrangian concentration field (coarse-grained over a scale r) is defined around *each* particle in the system by simply counting the number of particles $N_L(r,t)$ in a ball of size r centered around a particle. The (dimensionless) Lagrangian concentration is then defined as: $c_r(t) = \dfrac{N_L(r,t)}{\langle N(r,t) \rangle}$, where $\langle N(r,t) \rangle$ is the Eulerian frame mean concentration. With this definition, the Lagrangian concentration around any particle is at least: $c_r(t) = \dfrac{1}{\langle N(r,t) \rangle}$.

From a physical point of view, measuring a concentration in the Eulerian frame may be more intuitive, but averaging a quantity over a set of Lagrangian particles is equivalent to averaging over space with a weight proportional to the particle density [17]. The relation between the moments of n_r and c_r is then:

$$\left\langle c_r^p \right\rangle = \left\langle n_r^{p+1} \right\rangle \tag{10}$$

This relation holds when the number of particles in the system is large and the value of r is small [16]. Likewise, the PDF's of n_r and c_r are related: $\Pi(c_r) = \Pi(n_r)n_r$, by the simple relation of all of the individual moments in Eq. (10).

Experimentally, it is much easier to obtain accurate results by using the Lagrangian field c_r, rather than n_r [17]. The two representations of the concentration field have been systematically checked to ensure that the results of the more accurate Lagrangian field c_r is consistent with the less accurate Eulerian field n_r, using Eq. (10). In the following analysis, the results are expressed in terms of the Lagrangian concentration field c_r, keeping in mind the simple relation expressed in Eq. (10).

In this study of the concentration field statistics, care has been taken to focus only on the steady-state properties. To this end, the low order moments of the concentration fields, such as the first moment $\left\langle c_r(t) \right\rangle$, were measured systematically as a function of time. These moments first grow during a time of the order of the large eddy turnover time (Eq. (7)), and then fluctuate around a limiting value. This allowed the transient effects to be clearly separated from the steady-state regime. The following results correspond exclusively to the steady-state regime.
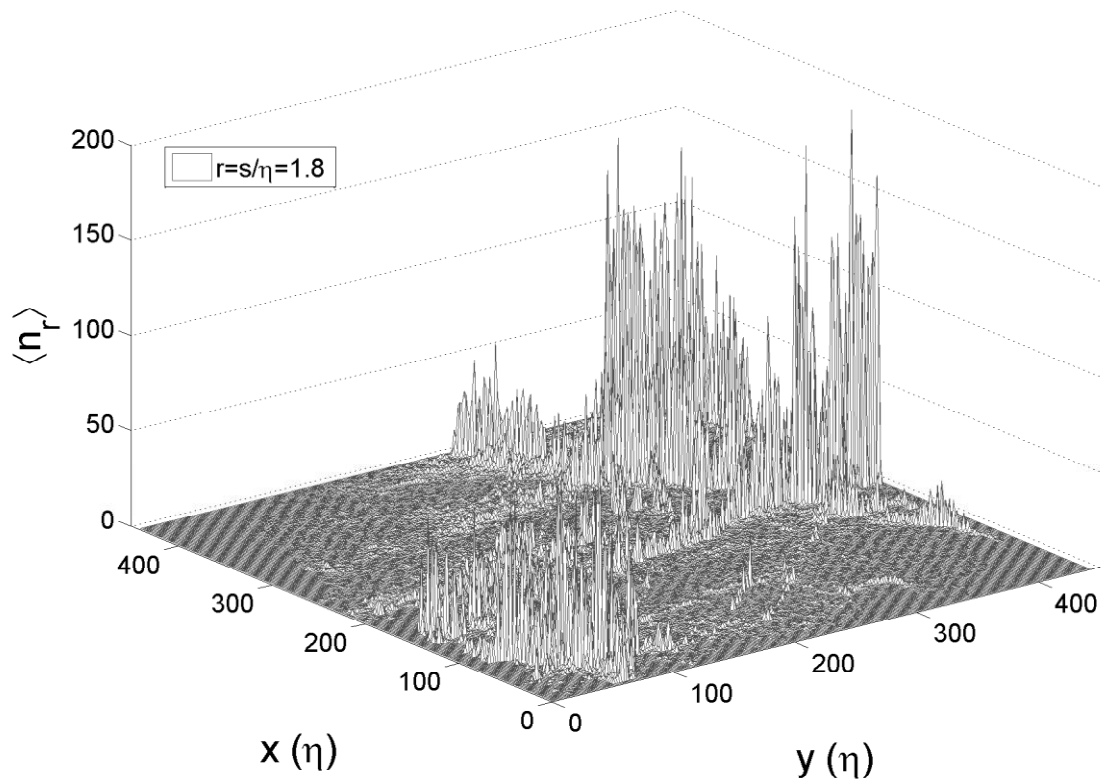
Figure 8: Visualization of the particle concentration field n_r **.** The Eulerian concentration field n_r in the statistically steady-state shows a very intermittent distribution, with very large spikes concentrated along string-like structures. Surrounding the string-like structure are (comparatively) depleted regions which are nearly flat. The *x* and *y* axes are in units of the dissipative scale η. The coarse-graining scale chosen here is *r*=1.8, which is in the dissipative range. Decreasing the coarse-graining scale *r* increases the intermittent nature of the particle concentration, and vice versa for increasing *r*.

2.3   RESULTS

2.3.1   Analysis

The results of the steady-state distribution of the coarse-grained particle concentration c_r are discussed in this section. The first result is the lowest non-trivial moment: $\langle c_r \rangle$, and its dependence on the dimensionless coarse-graining scale r [11]. The existence of a scaling relation, such as:

$$\langle c_r \rangle \sim r^{-\alpha} \tag{11}$$

Provides a characterization of the area where particles accumulate [17]. For simple geometrical structures such as points, lines, and surfaces, the scaling exponent α takes on the simple integer values $\alpha = 2,1,0$, respectively. For more complicated structures, as in the present case, the value of α is a non-integer and gives a quantitative measure of the complex topological structure. Systems with non-integer scaling exponents α are normally referred to as fractals, and in dynamical systems these fractal objects are called Strange Attractors [23].

Figure 9 shows that $\langle c_r \rangle$ exhibits two different scaling regions, at small ($r \leq 3.4\eta$) and at larger scales ($r \geq 5\eta$), which corresponds to dissipative and inertial ranges, respectively. These data can be fit with an exponent $\alpha_d \approx 0.92$ in the dissipative range and $\alpha_i \approx 0.79$ in the inertial range. The difference between the two scaling domains can be best seen by plotting the derivative $d\ln\langle c_r \rangle / d\ln r$ (see the inset of Figure 9). The qualitative impression from Figure 7 and Figure 8, that the result of the coagulation process is line-like structures, is completely

consistent with the values of the exponents $\alpha_{i,d}$ being close to 1. Higher order moments of the coarse-grained concentration also exhibit unique scaling in the inertial and dissipative ranges, transitioning between the two scales at approximately 5η. The results here are thus in qualitative agreement with the observations of [12] for $\langle n_r^{\,2} \rangle$, which also shows two separate scaling regions corresponding to inertial and dissipative ranges.
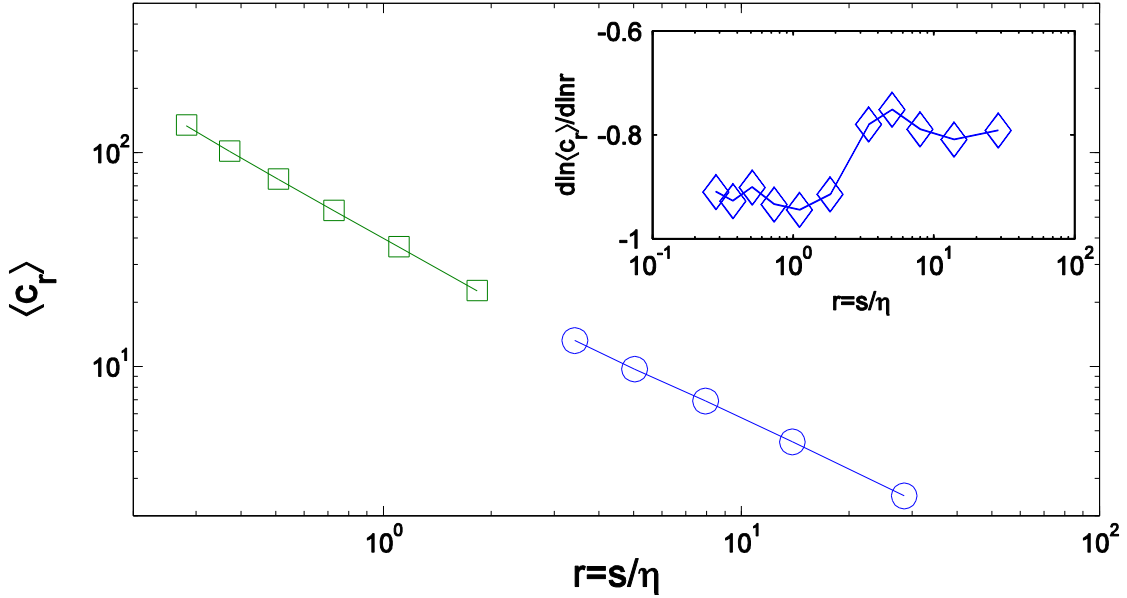

Figure 9: First moment of the Lagrangian concentration field c_r. The average $\langle c_r \rangle$ exhibits two scaling regimes. In the dissipative range, for $r < 5$, $\langle c_r \rangle$ scales as $r^{-\alpha_d}$ with $\alpha_d \approx 0.92$, whereas for $r \geq 5$, it scales as $r^{-\alpha_i}$ with $\alpha_i \approx 0.79$. The inset shows the derivative $d\ln\langle c_r \rangle / d\ln r$ and demonstrates the quality of the reported power-law behavior.

Next, the probability distribution function (PDF) of the Lagrangian concentration field $\Pi(c_r)$ is examined in both the inertial and dissipative ranges. Figure 10 shows the PDF (normalized by the mean concentration $\langle c_r \rangle$) in the dissipative range of scales r, while Figure 11 shows the PDFs in the inertial range. In the inertial range, and for r=3.4 in the dissipative range, the PDFs display a clear maximum in the distribution, with this maximum occurring at smaller values of $c_r / \langle c_r \rangle$ as r decreases. For values of $c_r / \langle c_r \rangle$ less than this maximum, the PDFs exhibit a plausibly linear behavior: $\Pi(c_r) \propto c_r$, which corresponds to a PDF in the Eulerian frame $\Pi(n_r) \propto const.$ (see Eq. (10)). This ensures that the PDF is normalizable in both the Lagrangian and Eulerian frames.

The very small $c_r / \langle c_r \rangle$ wing of the PDF is not observed deep in the dissipative range, for $r \leq 1.1$, due to the fact that values of $c_r / \langle c_r \rangle$ corresponding to less than one particle are not resolved (these calculations were carried out with $N_t \sim 4 \times 10^5$ particles). If the value of N_t is doubled, the power-law range of the PDF's for $r \leq 1.1$ is extended to smaller values of the concentration $c_r / 2\langle c_r \rangle$. This does not affect the power-law region of the PDF's discussed below, or the positive moments $\langle c_r^p \rangle$ for $p \geq 1$, which are dominated by the behavior of the PDF's at large $c_r / \langle c_r \rangle$.

The most interesting aspect of the PDFs in both ranges is the power-law behavior at values of $c_r / \langle c_r \rangle$ greater than the PDF's maximum, which correspond to the depleted concentration regions lying between the string-like structures in Figure 7 and Figure 8. In both ranges, the PDFs can be characterized by a power-law behavior: $\Pi(c_r) \propto c_r^{-\beta_r}$, over a limited range of $c_r / \langle c_r \rangle$ followed by a faster than algebraic cut-off at large $c_r / \langle c_r \rangle$ (see the insets of

27

Figure 10 and Figure 11). The variation of the exponent β_r characterizing the algebraic behavior in the dissipative range (Figure 10) is very small: $\beta_r \approx 0.8 \pm 0.05$ for $r \leq 3.4$. In comparison, the exponent β_r decreases when the scale r increases in the inertial range (Figure 12), with $\beta_r \cong 0.5$ at r=28.6 and $\beta_r \cong 0.75$ at r=5.0. The faster than algebraic decay of the PDFs in both ranges (inset of Figure 10 and Figure 11) ensures that all the moments of the distribution $\langle c_r^p \rangle$ exist for all $p \geq 1$. The observed cut-off is plausibly exponential over a limited range of large $c_r / \langle c_r \rangle$, before the PDF drops off to zero. The extent of the exponentially decaying range increases when the scale r decreases. The power-law decay corresponds to particle concentrations with an average spacing much larger than the particle radius a (2.2.1). Thus, surface tension effects play a negligible role in the formation of the power-law behavior.
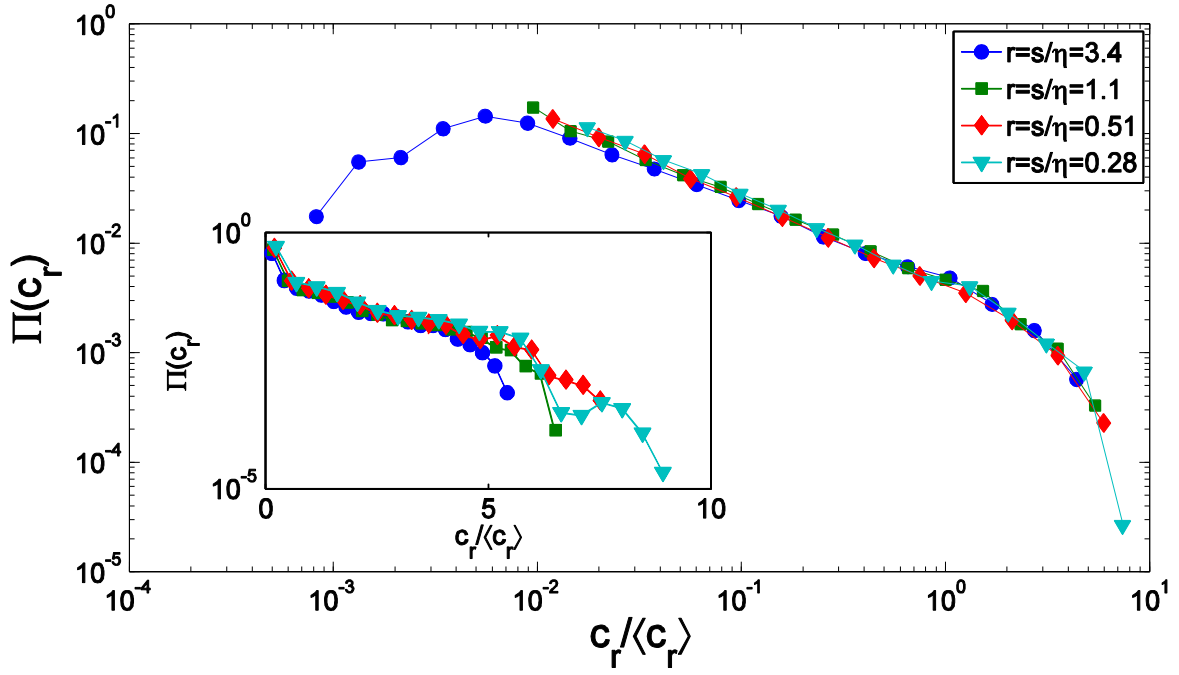
Figure 10: Probability distribution $\Pi(c_r)$ in the dissipative range. The PDFs of the concentration, scaled by the mean value $\langle c_r \rangle$, exhibit a power-law distribution at low values of $c_r / \langle c_r \rangle$: $\Pi(c_r) \propto c_r^{-\beta_r}$ with $\beta_r \approx 0.8 \pm 0.05$ (approximately independent of scale r). The PDFs decay faster than algebraically for $c_r / \langle c_r \rangle \geq 1$, see inset. The observed cut-off is plausibly exponential, over a range of $c_r / \langle c_r \rangle$ that grows when the scale r decreases.
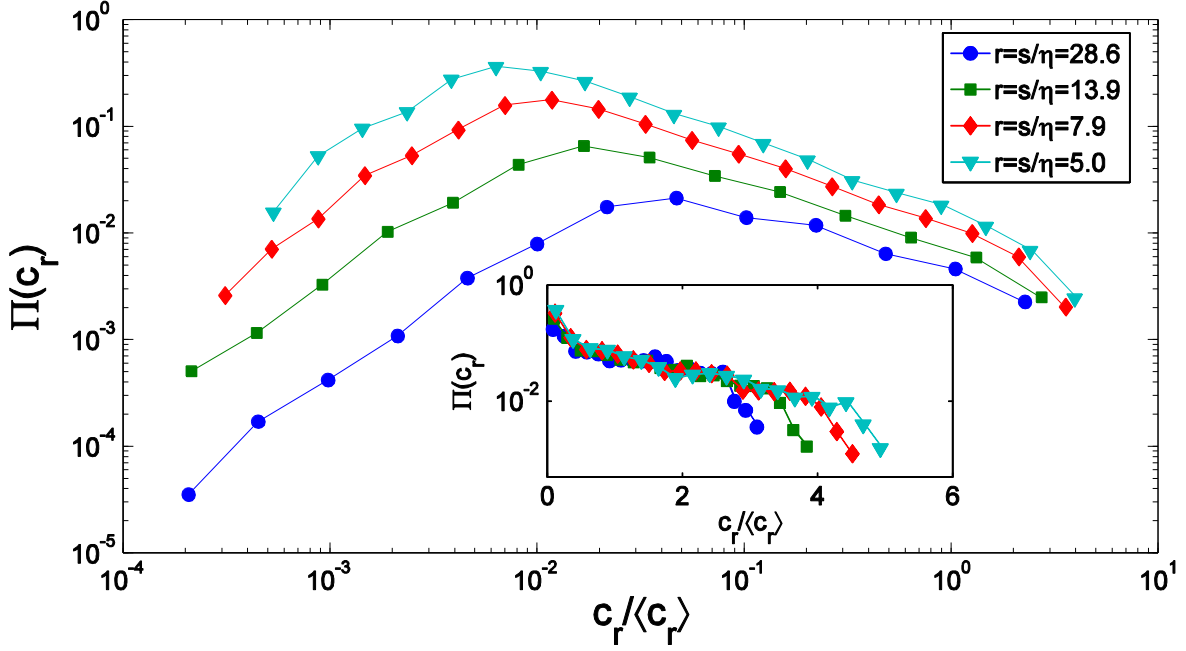
Figure 11: Probability distribution $\Pi(c_r)$ in the inertial range. The PDFs of the concentration scaled by the mean $\langle c_r \rangle$, exhibit a power-law distribution at low values of $c_r / \langle c_r \rangle$ greater than the PDF's maximum: $\Pi(c_r) \propto c_r^{-\beta_r}$, where the exponent β_r decreases when r increases. Here, $\beta_r \cong 0.5$ at r=28.6 and $\beta_r \cong 0.75$ at r=5.0. The PDFs decay faster than algebraically for $c_r / \langle c_r \rangle \geq 1$, see inset. The range of $c_r / \langle c_r \rangle$ where the exponential decay is observed shrinks when the scale r increases. The PDFs in the main figure have been shifted vertically to see the evolution of the power-law region.
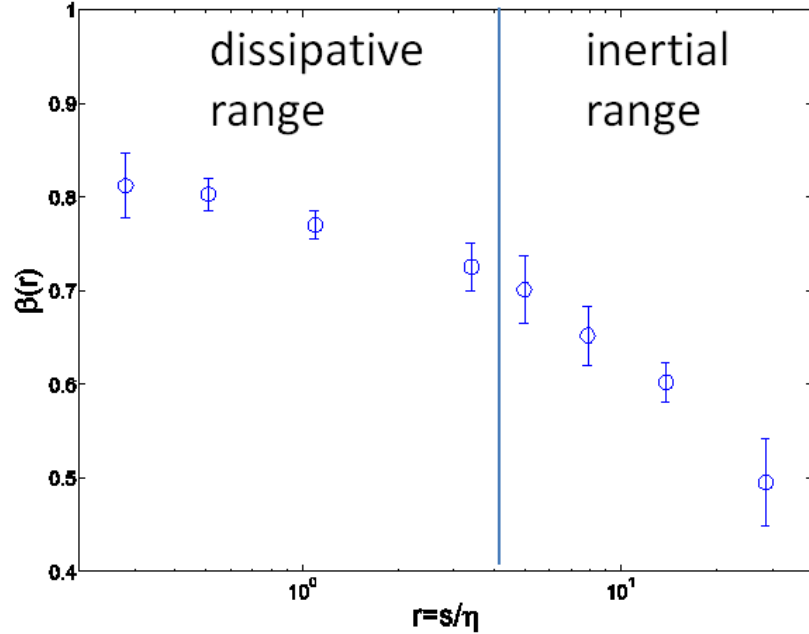
Figure 12: Exponent β_r as a function of scale r. The exponent characterizing the power-law behavior of the PDFs varies with scale r in the inertial range and is approximately constant in the dissipative range.

2.3.2 Discussion

The first important result of this work is the first moment of the particle distribution $\langle c_r \rangle$, which exhibits two different scaling regimes in the dissipative and inertial ranges for scales smaller and larger than $\sim 5\eta$. The existence of an inertial range scaling regime is qualitatively consistent with [12] for $\langle n_r^2 \rangle$, which also showed two scaling regimes in the inertial and dissipative ranges, with $\alpha_d > \alpha_i$ also. This numerical study used a "synthetic" turbulent flow model which allowed the compressibility C to be adjusted freely. The compressibility in this experiment is not a free parameter, and so the quantitative results of [12] cannot be compared usefully.

31

The PDF's in both ranges show a systematic evolution of the shape of the PDF of $c_r / \langle c_r \rangle$ as a function of scale r, qualitatively similar to the evolution of the velocity increment PDF in turbulence [18]. In the dissipative range, this observation is consistent with the theoretical arguments of [7], leading to the prediction that the particle distribution is multi-fractal. A multi-fractal distribution is defined by the scaling exponents of the moments of the concentration distribution $\langle c_r^p \rangle \propto r^{-\alpha_p}$. For a multi-fractal distribution, $\alpha_{p+1} \neq p\alpha_1$. This relation is implied if the PDF of the concentration *depends* on the coarse-grained scale r.

Consider a distribution for the Eulerian concentration which is *not* a function of r, $\Pi(n_r) \neq f(r)$. If there then exists a scaling relation of one of the moments $\langle n_r^p \rangle \propto r^{-\alpha_p}$, then every $2p_{th}$ moment $\langle n_r^{2p} \rangle \propto r^{-p\alpha_p}$, which is not a multi-fractal by definition. However, if the PDF's *are* functions of the coarse-grained scale r, $\Pi(n_r) = f(r)$, and a given moment of the distribution has a scaling relation $\langle n_r^p \rangle \propto r^{-\alpha_p}$, then $\alpha_{p+1} \neq p\alpha_1$ for all other moments. This result then proves the distribution is a multifractal. This same argument applies to the Lagrangian concentration c_r by Eq. (10).

The change of the PDF shape with r mostly affects the large $c_r / \langle c_r \rangle$ behavior where the PDF decays faster than algebraically, and also the pre-factor of the algebraic behavior, see Figure 10 and Figure 11. When the PDFs are re-expressed in terms of the Eulerian distribution n_r, $\Pi(n_r) \propto n_r^{-(1+\beta_r)}$, which are not even normalizable when $n_r \rightarrow 0$. Such a behavior has been observed in [9] with $\beta_r = 1$. The exponent β_r in this study varies systematically with scale r and is clearly different than the caustic prediction of $\beta_r = 1$ [9] (see Figure 10 and Figure 11). It is well known that solutions to the Burger's equation will produce shocks in the velocity field [24].

These shocks can produce divergences of a passive scalar field whose PDF will have power-law behavior(s) of $\Pi(n_r) \propto n_r^{-2}$ and $\Pi(n_r) \propto n_r^{-3}$. Although the resulting power-law behavior in the dissipative range in this work is close to $\Pi(n_r) \propto n_r^{-2}$, it is measurably different. It is also unlikely that the results in this work are due to caustics [21], since the particles here follow the measured flow field directly by Eq. (9), which is presumably governed by the full 3D Navier-Stokes equation.

The theoretical work in [20] predicts a power-law behavior of the coarse-grained concentration n_r in the dissipative range, $\Pi(n_r) \propto n_r^{-(1+\beta_r)}$, with $\beta_r < 0$, which ensure that the distribution is normalizable. This is consistent with the results in this work for the PDF at r=3.4, see Figure 10, which shows $\Pi(c_r) \propto c_r$, corresponding to a PDF in the Eulerian frame $\Pi(n_r) \propto const.$. The PDFs in this work for intermediate values of n_r (or c_r) in the dissipative range, display power-law behavior with $\beta_r > 0$. This does not strictly violate the prediction in [20], since the smallest concentrations are not resolved for r<3.4.

3.0   CONCLUSION

In order to characterize the statistical properties of particle clustering on the surface of a turbulent flow, the coarse-grained particle concentration c_r around *each* particle in the system in a domain of size $\sim r^2$ has been measured, normalized by the expected particle concentration in the case of a homogeneous system. This study has covered a range of scales extending from the dissipative up to the inertial range scales. The first moment of the particle distribution $\langle c_r \rangle$ exhibits two different scaling regimes in the dissipative and inertial ranges, for scales smaller and larger than $\sim 5\eta$. The PDF of c_r vary systematically with scale r. This is consistent with a multi-fractal particle distribution in both the inertial and dissipative ranges, which is generally consistent with the findings of [12]. The PDFs exhibit power-law behavior at small $c_r / \langle c_r \rangle$, characterizing the broad concentration distribution of particles contained in areas between the line-like structures formed by surface sinks. When the PDFs are re-expressed in terms of the Eulerian distribution n_r, $\Pi(n_r) \propto n_r^{-(1+\beta_r)}$, which are not even normalizable when $n_r \to 0$. Such a behavior has been observed in [9] with $\beta_r = 1$, while the exponent β_r in this study varies systematically with scale r and is clearly different than the caustic prediction in [9] of $\beta_r = 1$. This work thus indicates that the intermittent distribution of particles in free-surface flows is characterized both by very high particle concentration along string-like sinks, as well as by a strong depletion of particles near fluid sources. A proper description of the resulting power-law

tails requires a better understanding of the very efficient expulsion mechanism of particles from large regions of the turbulent surface flow. The proper understanding of this mechanism which leads to particle clustering is of both fundamental interest and practical use in understanding transport phenomena on the surface of turbulent flows.

3.1 FUTURE WORK

The results of this work have (in the author's opinion) thoroughly probed the important length and time scales which are important to free-surface turbulence. However, the Re_λ achieved in this experiment (~100) is rather modest compared to other more turbulent flows [18]. Most theoretical work in turbulence is made possible by considering the limit that $\mathrm{Re}_\lambda \to \infty$ (or equivalently, $\upsilon \to 0$) [18]. It is thus likely that any further theoretical advancement of this flow type will require the asymptotic limit $\mathrm{Re}_\lambda \to \infty$.

However, the amplitude of surface waves is difficult to control with increasing velocity fluctuations. A more effective exercise may be to perform an experiment at the surface *without* minimizing the surface waves. In most practical situations, surface waves are likely to play a role in surface concentrations, as they did in [9]. One might then perform an experiment in an apparatus which produces *both* 3D incompressible turbulence in the tank's bulk *and* waves at the surface, through some controlled mechanism. The two mechanisms may then be studied together. The surface wave's amplitude and frequency could be controlled as they are in [9]. The surface compressibility ($C \approx 1/2$) is not controllable, as noted in [5].

Studying *inertial* particles which are buoyant would also be of fundamental interest. It would be difficult to satisfy both inertial and buoyancy requirements simultaneously. It's likely that these particles would need to be hollow (buoyant), which would require the particle's diameter to be larger than the dissipative scale η (inertial) to produce a large enough stokes number St to be considered inertial. In doing so, one would lose the theoretical predictions for the particle distribution inside the dissipative scale [2,7].

It would also be interesting to study how the distribution of particles changes for decaying turbulence at the surface. Imagine that the particle distribution is driven into a steady state by a turbulent tank. Then, the turbulence would be shut off and the distribution of particles would be tracked. Assuming that the line-like structures are preserved during the decay of turbulent motion, these coagulations would be subject to Brownian diffusion. They would then be stable for a time which is much larger than the turbulent time scales in this experiment. The purpose of such an experiment would be to analyze how the correlated turbulent flow which produces these coagulations decays in time. If the correlated flow structure which produced the coagulations is not preserved during the decay, the coagulations may disperse in a time comparable to the turbulent time scales of this experiment.

Another interesting experiment would be to track very dense particles which are confined to the *bottom* of the tank. There they would also be subject to a turbulent flow which is driven by the bulk 3D incompressible turbulence. It can be shown [6] that any 2D slice of a 3D turbulent incompressible flow will have a compressibility $C = 1/6$. Thus, heavy particles which are free to move along the turbulent tank's bottom should also cluster, in principle. This could help understand the transport of sediment at the bottom of lakes, rivers, etc.

4.0   ACKNOWLEDGEMENTS

BIBLIOGRAPHY

[1] R.A. Shaw, Annu. Rev. Fluid Mech. **35**, 183 (2003).

[2] G. Falkovich, A. Fouxon, and M.G. Stepanov, Nature **419**, 151 (2002).

[3] L.F. Richardson, Proc. Roy. Soc. A **110**, 709 (1926).

[4] H. Stommel, J. Marine Res. **8**, 199 (1949).

[5] J.R. Cressman, J. Davoudi, W.I. Goldburg, and J. Schumacher, New J. Phys. **6**, 53 (2004).

[6] G. Boffetta, J. Davoudi, B. Eckhardt, and J. Schumacher, Phys. Rev. Lett. **93**, 134501 (2004).

[7] J. Bec, K. Gawedzki, and P. Horvai, Phys. Rev. Lett. **92**, 224501 (2004).

[8] G. Boffetta, J. Davoudi, and F. DeLillo, Europhys. Let. **74**, 62 (2006).

[9] P. Denissenko, G. Falkovich, and S. Lukaschuk, Phys. Rev. Lett. **97**, 244501 (2006).

[10] M.M. Bandi, W.I. Goldburg, and J.R. Cressman, Europhys. Lett. **76**, 595 (2006).

[11] M.M. Bandi, W.I. Goldburg, and J.R. Cressman, J. Stat. Phys. **130**, 27 (2008).

[12] L. Ducasse and A. Pumir, Phys. Rev. E **77**, 066304 (2008).

[13] G. Falkovich and A. Pumir, Phys. Fluids **16**, L47 (2004).

[14] G. Falkovich, A. Weinberg, P. Denissenko, and S. Lukaschuk, Nature **435**, 1045 (2005).

[15] G. Boffetta, F. DeLillo, and G. Gamba, Phys. Fluids **16**, L20 (2004).

[16] E. Balkovsky, G. Falkovich, and A. Fouxon, arXiv.chao-dyn p. 9912027 (1999).

[17] P. Grassberger and I. Procaccia, Phys. Rev. Lett. **50**, 346 (1983).

[18] U. Frisch, Cambridge University Press (1996).

[19] M.E.J. Newman, Contemporary Phys. **46**, 323 (2005).

[20] E. Balkovsky, G. Falkovich, and A. Fouxon, Phys. Rev. Lett. **86**, 2790 (2001).

[21] M. Wilkinson and B. Mehlig, Europhys. Lett. **71**, 186 (2005).

[22] P. Yeung and S. Pope, J. Comp. Phys. **79**, 373 (1988).

[23] J. R. Dorfman, Cambridge University Press, 1999.

[24] J. Burgers, Dordrecht, Amsterdam, 1974.

[25] S. Pope, Cambridge University Press, 2000.